Hearing the Shape of the Universe:

A Correlation Matrix Search of Oblique Cosmic Torus Topologies

John Dulin
Adviser: Dr. Glenn Starkman

May 1, 2015
Revised May 18, 2015

Contents

1 Introduction **1**
- 1.1 Candidate Spaces . . . 1
- 1.2 The Fundamental Domain and Tiling . . . 3
- 1.3 Background and Previous Work . . . 4
- 1.4 Theory . . . 7
  - 1.4.1 The Laplacian Eigenmode Problem . . . 7
  - 1.4.2 The Correlation Matrix . . . 8

2 Multiconnected Space Eigenmode Solutions **10**
- 2.1 Solving for the Laplacian Eigenmodes . . . 10
- 2.2 Solving for Oblique Spaces . . . 11
- 2.3 Candidate Space Solutions . . . 13
  - 2.3.1 Oblique 3-Torus . . . 13
  - 2.3.2 Oblique Half Turn Space . . . 13
  - 2.3.3 Oblique Quarter Turn Space . . . 14

3 Generating the CMB Sky **16**
- 3.1 Expansion in Terms of the Full-Sky . . . 16
- 3.2 Observable Mode-Mode Correlation Matrix . . . 17

4 Summary **22**

Abstract

Previous work discerning the topology of the universe has focused on methods like cosmic crystallography and circles-in-the-sky searches, as well as examinations of the correlation matrix to uncover manifolds with non-trivial topology. While helping to constrain the universe's possible topologies, these investigations have not discovered the ultimate universal shape. This project aims to extend that investigation to a broader set of topological spaces, oblique-torus topologies, using the known correlation function comparison method. This comparison identifies correlations of temperature intensity in the CMB sky which would be uniquely induced by multiconnected topologies.

In order to apply this idea to the three-manifold of the universe and its CMB, we tiled the universe at the time of last scattering with the solutions of the Helmholtz equation for a scalar field on candidate topologies. These eigenmodes of the Laplacian describe the the time-independent standing wave solutions of radiation for a shape in question, and therefore any topology-induced anisotropies of temperature in the CMB. To test candidate topologies, we then derive a general solution for the correlation matrix of candidate topologies. This can simulate candidate spaces of arbitrary size and angular slant with the ultimate goal of finding a single statistically significant correlation between simulated CMB anisotropies and observed Planck data.

Chapter 1

Introduction

1.1 Candidate Spaces

One of the most fundamental questions of cosmology is "What is the shape of space?" More formally, "What is the geometry and topology of space?" At first, this question seems so broad that beginning to answer it is difficult. The universe is enormous, as is the number of possible three-dimensional shapes, and physicists cannot directly observe the shape within which we live. There are no known methods to analytically predict cosmic topology, as that would be a consequence of a quantum gravity theory. [1] [1]

However, a useful quality of such fundamental questions is that their set of possible solutions can be pruned with fundamental assumptions. We have powerful classifications of shapes both topologically and geometrically from mathematics. We begin our search by prioritizing three-dimensional spaces by the qualities we would require them to produce in physical phenomena. That is, answering the question "What shapes could exhibit the observable phenomenon (In large scale structure, the CMB, etc.) we perceive in the universe?" So, our search for a universal shape becomes just that: A search on the set of possible topologies for one which would be exclusively responsible for some statistically significant experimental qualities in the observable universe.

With our current cosmological understanding, we are able to build a reasonably small set of candidate topologies by requiring certain qualities from space. The universe is (usually) defined as a differential manifold, as space is assumed to be differentiable and continuous. It is then required to coincide with the apparent isotropy and homogeneity observed in the mass and energy distribution of the universe and have constant properties throughout time. This prioritizes shapes of constant curvature. Shapes without boundary are prioritized because we do not have a physical description for a boundary of the universe. Although

[1] By this we mean a cosmic topology cannot be solved for directly with just "pen and paper." The cases of certain non-trivial topologies can theoretically be confirmed or refuted experimentally though, which is the work this project contributes to [2].

we do not know if the universe is finite or infinite, the logically awkward conclusions of an infinite universe [2] and the difficulty of learning whether it is finite lead us first to consider finite, multiconnected topologies. Multiconnected topologies are shapes with holes, or disconnections, in the connectedness of their domain which prevent all closed loops from being pulled to a point. This creates distinct sets of loops which represent the connectedness of a space based on which disconnection they may be pulled about. The simply-connected topology (A completely connected topology on which any closed path can be pulled to a point.) is trivial and, for a finite universe, could be considered the "null case" of these non-trivial topology searches [2]. These loops are illustrated in Figure 1.2, where loops a and b illustrate the different paths around the disconnection of the donut's hole and loop c illustrates a loop drawn on a topologically trivial submanifold of the torus.

These considerations restrict our set of candidate topologies to compact, multiconnected spaces of constant curvature without boundary. Through these constraints, a set of possible topologies is created. Many shapes are given priority on ascetic and practical grounds. Through their anticipated qualities, a set of methods to test cosmological data for candidate shapes is built. Ideally, we want these experimental tests to have a one-to-one and onto mapping between candidate topologies and observations. I.e.: The test should be able to uniquely identify one cosmic space through experiment so that all other possible spaces are ruled out.

The cosmic microwave background (CMB) and spectral geometry provide such a test. The CMB is the oldest snapshot we have of the universe: The radiation which emanated from a 2-sphere called the last scattering surface (LSS) - The last surface from which photons were emitted as thermal radiation from the primordial universe, about 380,000 years after the Big Bang [2]. It theoretically carries the most information of our universe's shape as it is the largest scale on which we can probe cosmic topology [8].

Conveniently, there is a mathematical description of the radiation of the CMB anisotropy which forms a bijective mapping between observations of the CMB and our candidate flat, multiconnected topologies: The eigenspectrum of the Laplacian with unique boundary conditions for a given candidate shape. [3] This is the inverse problem of spectral geometry - Identifying the qualities of a geometry from its eigenvalue spectrum. The problem is often posed as "Can you hear the shape of a drum?" Can the discreteness of sound waves heard elucidate the shape of a drum? In our case, can the discreteness of the CMB radiation illuminate the shape of the universe? The answer to this question is "Yes" in our case, as the 17 candidate flat spaces on non-trivial topology have unique eigenspectrums [11]. While it is possible the universe is none of these spaces or we cannot acquire topological information from the CMB for other

[2] As Levin explains, "By the law of probability an infinite universe accommodates an infinite number of events each happening an infinite number of times. Somewhere else in the cosmos, you are there." [1]

[3] Although the universe appears quite flat, there is a possibility it is elliptically or hyperbolically curved. These are less likely and more difficult cases to study though.

Figure 1.1: A multiconnected two-torus of a two-dimensional manifold with examples from each of the three distinct sets of topological loops on its surface.

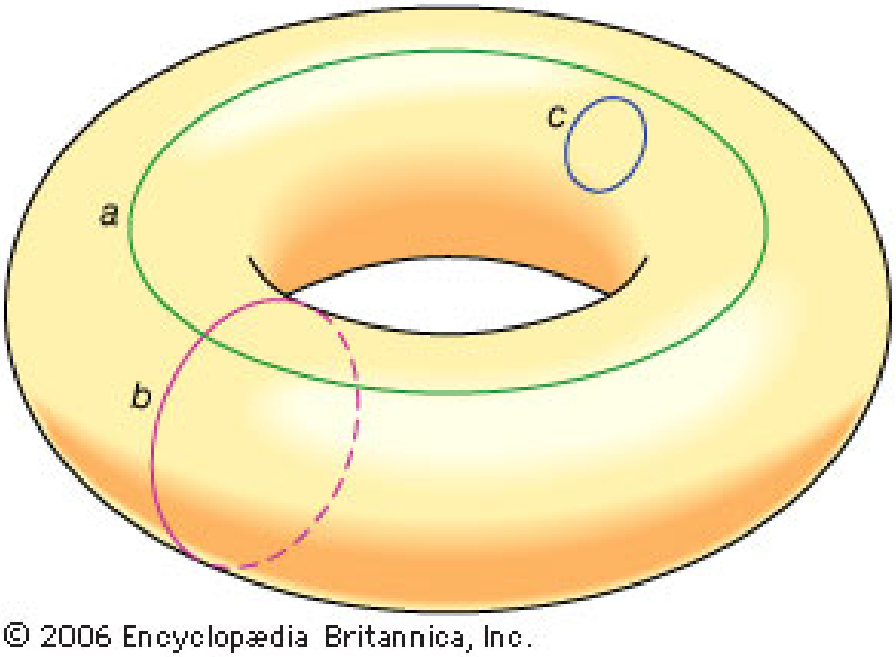

reasons, we can at least rule out these as candidates within the known limits of our methods. These assumptions form the basis of the correlation matrix search for a cosmic topology we are pursuing in this report.

1.2 The Fundamental Domain and Tiling

First, it is important to describe our mathematical conceptualization of multiconnected spaces like the three-torus. In a torus topology, the connectedness is seen intrinsically (Within the space.) as a loop: To observers within the topology, travelling in a straight line far enough will eventually bring us back to where we started. In a multiconnected torus topology, this can be done in several directions (In the case of a three-torus, every direction.). [11] The best way to first imagine this is in a two-dimensionally multiconnected torus topology, like that of the "donut" torus in Figure 1.2.

This connectedness (Shown in the loop paths on Figure 2.1.) is the way we imagine finite (In 1, 2, or 3 dimensions.) universes without boundary. So, our searches for non-trivial topologies often try to observe distinctive traces of this connectedness from edges of a finite universe. Mathematically, we conceptualize this connection around dimensions as creating 'clones' of our universe which we can reach if we travel far enough. This is not to say there are multiple

Figure 1.2: An example of a two-dimensional Klein bottle torus topology fundamental domain embedded in a covering space. Connected sides have the same marks on their delimiting lines.

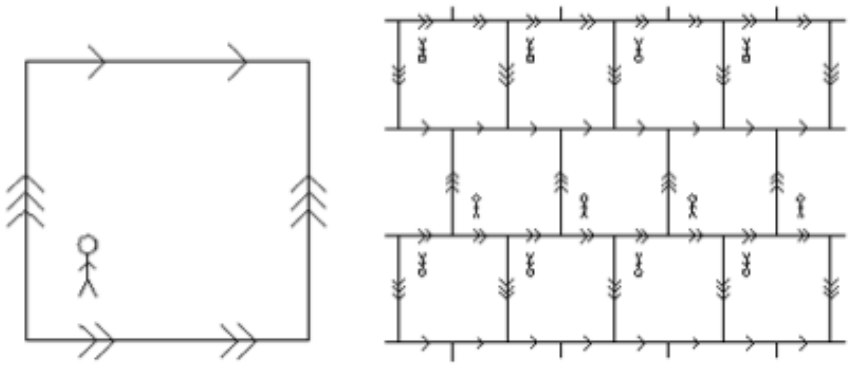

universes - There is only one, finite universe. But, we can imagine the connectedness by imagining an infinite, simply-connected three-dimensional universe with the constant curvature of our universe (Called the covering space.) filled (Or "tiled.") by repetitions of the finite shape of the actual universe (Called the fundamental domain.). To clarify, the fundamental domain (fundamental domain) is the only *real* universe, but filling a mathematical covering space with copies of the fundamental domain where the connected edges of each fundamental domain are bijectively mapped together is a useful way to imagine the way physical phenomena can be perceived across multiple fundamental domains. This is illustrated in Figure 1.2. Across the boundaries linked, the stick-figure character can see the other copies of herself like in a mirror.

The crucial feature of this tiling of space is that it creates periodicity in the covering space. This is true for matter, mathematical translations between tiles, and eigenmodes of radiation filling space. These tiles and translations between them are described by group generators Γ which are periodic spatial translations between identical points in each tile. The group generator is unique to each space, an important quality we will use later. This useful conceptualization of a group generators g translating between two tiled fundamental domains is shown for two-dimensions in Figure 1.2.

1.3 Background and Previous Work

As physicists acquire the experimental tools to probe nature for the universe's geometry and topology, a collection of unique methods for testing candidate shapes was built. Often, these only work under in topological or geometric situations. However, trying and failing to find the universal topology with these methods has succeeded in further constraining the type or size of our univer-

Figure 1.3: A group translation g between two identical points in a two-dimensional universe, but connected across a tile.

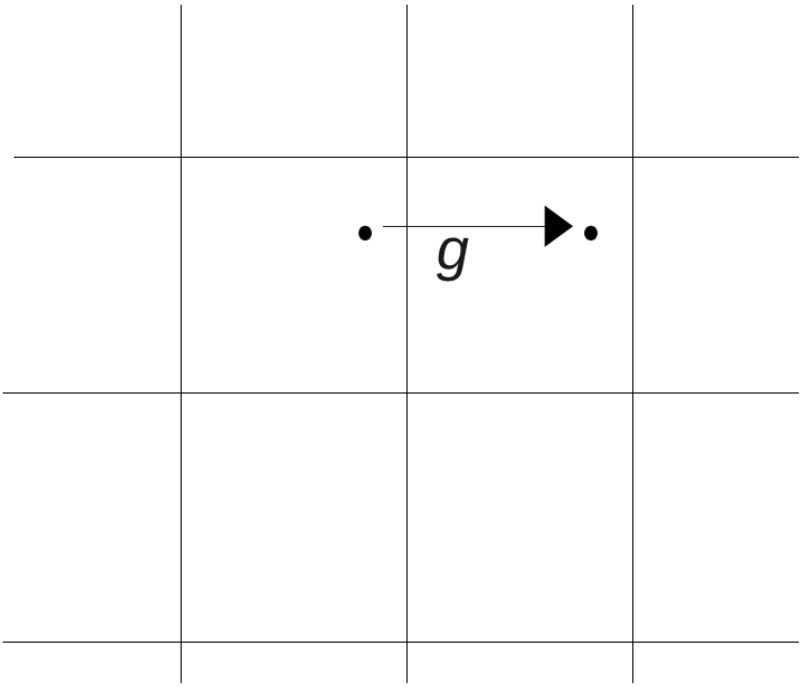

sal shape by supporting null hypotheses bounded by the limits of a method's theoretical ability to distinguish different spaces. Three of these methods used in the past; cosmic crystallography, circles-in-the-sky, and correlation matrix examinations, are described below, although crystallography is believed to be largely exhausted as a source of cosmic topology research.

The earliest searches for a non-trivial topology scanned the astronomical sky for repeated patterns of galaxies [8] [5]. These searches attempted to discern a torus topology by the number and amplitude of repeated galaxy clusters (Which would be visual 'clones' of the same physical galaxies.) captured in the radius of the visible universe. The method is called 'cosmic crystallography' because the patterns this looks for in a tiling of fundamental domains are similar to that of an atomic crystal lattice [5].

The quantification of the crystallography search is the pair-separation histogram (PSH): A graph of the number of occurrences of distance magnitudes between two distant light sources in the sky. If there are no repeat images, this is a Poisson probability distribution. If there are, "spikes" will appear in the histogram which denote repeated patterns of images coming from multiple fundamental domains. Each of these images would be an isometry translation of another - A translation in space preserving distance between a pair of galaxy clusters and their clone in another fundamental domain. In Euclidean and elliptic geometries, these translations mean that the observed distances between galaxy clusters will be the same even though the clusters appear in different places [9]. Thus, we can count the occurrences of certain distances between astronomical structures and infer significance from anomalous counts.

However, this method only finds a topology if the radius of the visible universe [4] is large enough to encompass several of these galactic structures in multiple fundamental domains. It is also unable to perceive hyperbolic spaces because the translations between their fundamental domains are not isometries. Multiple shapes may even produce identical spike patterns in the PSH. Ultimately, searches for cosmic crystallography patterns have not yielded any evidence of a non-trivial topology. They did however begin to place lower bounds on the dimensions of a multiconnected flat space.

Another method, the search for "Circles-in-the-Sky", is a more general and powerful tool for identifying non-trivial topologies. This is because it is based on analysis of CMB data, which means it is not limited by the radius of the visible universe, as cosmic crystallography is. This method was first applied to COBE data [4], and was quickly applied to several more non-trivial topology searches [6].

The method is well-named, as it searches for pairs of matching circular patterns in the CMB anisotropy. These would denote intersections between the surface of last scattering between our fundamental domain and another. Their existence and qualities can then be used to infer (Or at least constrain.) the size and topology of the universe.

So what exactly are these circles and what would theoretically cause them?

[4] The three-dimensional ball of light which has reached us.

Figure 1.4: An Earth centered at the LSS will see two identical circles in the sky if the radii of the LSS (The orange spheres.) is larger than the smallest radii of the fundamental domain.

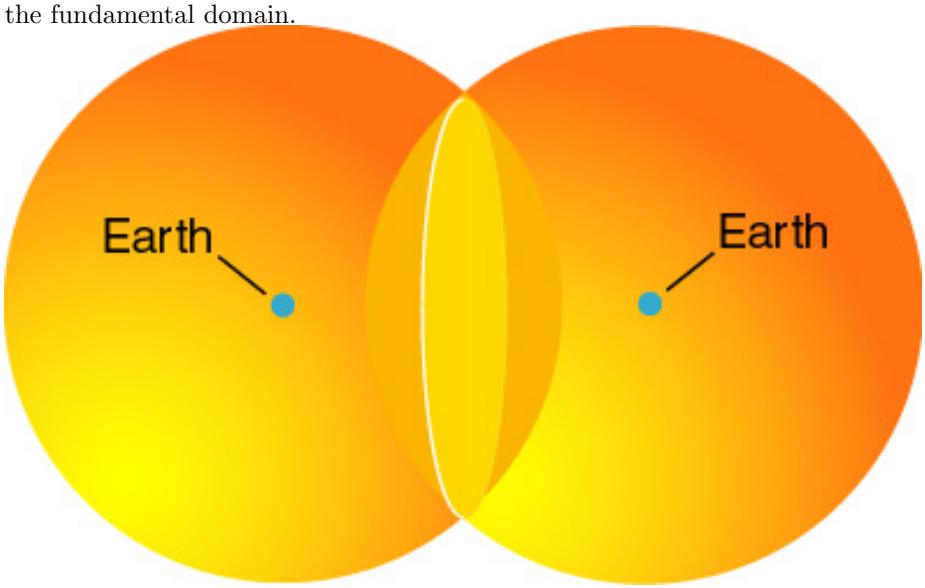

It is a phenomenon which would occur when the diameter of the LSS is greater than that of the smallest finite dimension of the fundamental domain. Like the light we would expect from distant galaxies in a visible universe with sufficiently large diameter, the CMB may "wrap around" and appear behind an observer if it is sufficiently large in front of them. As the LSS is a two-sphere, the viewer within the two sphere should be able to identity antipodal (At least in the case of the flat three-torus.) circles of matching anisotropy patterns from the intersecting surface area of the CMB radiation as it looped around the universe's connectedness. This is illustrated in Figure 1.3. While applications of this method did not find statistically significant evidence of a multiconnected topology, they have raised the lower bound of the universes lowest fundamental domain radius to approximately 26 Gpc [6].

1.4 Theory

1.4.1 The Laplacian Eigenmode Problem

The Helmholtz equation can be written

$$\nabla^2 \xi_n(\mathbf{x}) = \lambda^2 \xi_n(\mathbf{x}) \tag{1.1}$$

where $\xi_n(\mathbf{x})$ is the value of an independently-evolving wave indexed by eigenmode n at position $\mathbf{x}$ in flat space.

For flat, multiconnected topologies these will be linear combinations of plane waves

$$\xi_n = \sum_{j=1}^{b} \xi_{nj} e^{i\mathbf{k}_{nj}\cdot\mathbf{x}_p} \tag{1.2}$$

where ξ_{nj} is a term-specific coefficient. For the set of topologies we consider, b may equal either 1, 2, or 4 (The number of terms in the linear combination defining the eigenmode.). Note that the wave vectors depend both on n, the normal wave mode number, and j, the index of the unique plane wave term they come from.

Each of the planar waves $e^{i\mathbf{k}\cdot\mathbf{x}}$ of the linear combination is distinguished by the form of its wave vector. In Section 2.2 an algorithmic approach from Riazuelo et. al [11] is described for producing these from the unique generators of each topology. Coefficients are then given by enforcing the criteria

$$\xi_n(\mathbf{x})\xi_n^*(\mathbf{x}) = 1 \tag{1.3}$$

for eigenmodes ξ_n.

We solve for the dependence of $\mathbf{k}$ on the oblique angles of slanted spaces in Section 2.2. This comes from describing the basis vectors of such a fundamental domain, which is a parallelepiped for all of the spaces we examine here.

1.4.2 The Correlation Matrix

The distinct boundary conditions of multiply-connected topologies will produce subtle violations of global isometry and homogeneity in the angular power spectrum of the CMB. To identify these and how they will appear for any candidate space, we generate the simulated correlation matrix of angularly separated temperature values on the CMB. The correlation matrix provides all of the information of statistical correlations of intensity between points on the CMB by comparing each and every pixel with all others.

The entries of the theoretical pixel-pixel correlation matrix are the two-point correlation function of temperature between two pixels in the CMB sky,

$$C_{pp'} = \langle T_p T_{p'}^* \rangle \tag{1.4}$$

where temperature is

$$T(\mathbf{x}) = \sum_{n=1}^{\infty} a_n \xi_n(\mathbf{x}) \tag{1.5}$$

in the topology frame, a_n is a statistically-independent Gaussian random variable, the temperature intensity, and $\xi_n(\mathbf{x_p})$ is the space's respective Laplacian eigenmode. As described above, these are linear combinations of plane waves as in equation 1.2.

To be useful, the expression for temperature at a position in the topology frame must be expressed as a function of pixels in the CMB sky. So, pixels in the observer frame must be mapped to position points in the topology frame.

For any topology, the positions on the CMB sky are the same: Points on a sphere of radius $R_{\rm LSS}$, the distance to the last scattering surface, centered on the observer. Our relation of pixel space to topology space is then

$$\mathbf{x}_p = \mathbf{r}_T + R_{\rm LSS} R_{\alpha\beta\gamma} \hat{p} \tag{1.6}$$

where $\mathbf{r}_T$ is the position of the observer (Earth) in the topology frame and $R_{\alpha\beta\gamma}$ is the rotation matrix specified by Euler angles $(\alpha\beta\gamma)$ which places pixel $\hat{p}$ on the sphere. $\mathbf{x}_p$ is then the position of a pixel corresponding pixel p in the topology frame.

When we explicitly include this mapping in our temperature expression, equation 1.5 becomes

$$T(\mathbf{x}_p) = \sum_{n=1}^{\infty} a_n \sum_{j=1}^{b} \xi_{nj} e^{i\mathbf{k}_{nj}\cdot(\mathbf{r}_T + R_{\rm LSS} R_{\alpha\beta\gamma}\hat{p})}. \tag{1.7}$$

For any candidate topology, it's assumed that

$$C_n \delta_{nn'} = \langle a_n a_{n'} \rangle \tag{1.8}$$

and each term of each index in the correlation matrix is dependent only on the magnitude of each $\mathbf{k}_{nj}$,

$$C_n = C_n(|\mathbf{k}_{nj}|) = C|\mathbf{k}_{nj}|^{-p} \tag{1.9}$$

where p is some positive number. We select $p = 3$ as a good fit for the Harrison-Zel'dovich spectrum, although better fits may exist.

Our general pixel-pixel correlation matrix is then

$$C_{pp'} = \sum_{n=1}^{\infty} \sum_{n'=1}^{\infty} \langle |a_n^2| \rangle \delta_{nn'} \xi_n(\mathbf{x}_p) \xi^*_{n'}(\mathbf{x}_{p'}). \tag{1.10}$$

Chapter 2

Multiconnected Space Eigenmode Solutions

2.1 Solving for the Laplacian Eigenmodes

In this chapter we define the eigenmode solutions for three oblique topologies: The 3-torus, half-turn space, and quarter-turn space. These all share the basis of a parallelepiped. The full set of candidate flat multiconnected flat spaces is eighteen [11], however we have begun our examination of oblique spaces with the three simplest and most easily slanted of those. Future work would expand these solutions to consider the other fifteen spaces, applying the oblique transformations where possible.

The 3-torus is the simplest of the multiconnected topologies we consider: A rectangular prism with opposite sides glued (Connected topologically - Each point on the manifold of one face is mapped to the corresponding point of the other surface.). The half-turn torus and quarter-turn torus are derived from rotated gluings of opposite sides of the rectangular three-torus. The half-turn space is characterized by a 180°corkscrew rotation of the connection while the quarter-turn is a 90°rotation. (One face, when mapped over to another, is flipped once clockwise.) A 270°turn, while possible, is just a quarter-turn in the reverse direction and therefore has the same eigenmode solutions as the 90°quarter turn [11].

All Laplacian eigenmodes of multiconnected flat spaces are linear combinations of the eigenmodes of Euclidean flat space - planar waves $e^{i\mathbf{k}\cdot\mathbf{x}}$. These functions are in turn periodic eigenmodes of the Euclidean covering space. Because of this, we can produce the set of planar wave terms which make up the linear combination of a space's eigenmode by repeated application of the generator Γ. This is a spatial translation which produces the point it acts on translated across a fundamental domain boundary, through some dimension of the topology's connectedness [2].

These generators have both a rotation matrix factor R_a and spatial transla-

tion factor T_a for some dimension a,

$$\Gamma_a = T_a R_a \tag{2.1}$$

such that the position vector under a corkscrew rotation is,

$$\Gamma_a \mathbf{x} = R_a \mathbf{x} + V_a \tag{2.2}$$

where V_a is a spatial translation by a distance L_a, the distance across some dimension (In this case the z.) of the fundamental domain. R_a is defined to satisfy the boundary constraints. The unique planar wave terms of a multiconnected eigenmode are produced by applying this Γ to $\mathbf{k}$ instead of $\mathbf{x}$.

If this seems a precarious argument, there are several reasons why this generation of eigenmodes works. First, any Γ operation on $\mathbf{k}$ is equivalent to a spatial translation since the wave vector is in the dual space. Furthermore, this operation is closed on planar waves and we may select R_a such that it is of finite order b. This finite order should (For the boundary conditions of our candidate spaces.) make the R matrix closed under a periodic, b-dimensional space of eigenmodes which are the planar waves of the multiconnected space.

Our essential problem is then finding Γ periodic eigenmodes of Euclidean flat space. The simple algorithm described above makes the crux of this problem defining Γ for the space under consideration. After the forms of the distinctive $\mathbf{k}$s are found for the summed planar waves, we simply need to define a restriction of the eigenmode wave numbers n (To avoid repeat terms of certain planar waves.) and a normalization coefficient in accordance with 1.3.

The basic wave vector for all 3-torus topology spaces (Rectangular prism 3-torus, Half turn rectangular prism, quarter turn rectangular prism.) is

$$k_a = \frac{2\pi n_a}{L_a}, n_a \in \mathbf{Z}. \tag{2.3}$$

These wave vectors produce the twisted cases of the right rectangular prism cases with a generator $\Gamma = R_a$, as the twisted gluings only flip paths across the tiling. By itself, it is the allowed wave vector form for the right 3-torus.

Wave vectors 2.3 are kept as a basis for the twisted cases of the rectangular prism by shrinking the length of their fundamental domains so that the twisted spaces are considered subspaces of the untwisted. Then, repeated corkscrew rotations across several of these shrunken fundamental domains of a certain number (The generator modulus over the solution terms.) produce the original, untwisted fundamental domain. In other words, setting the distance $V_a = L_a/b$ for the modulus of the space b lets the 3-torus wave vector produce the twisted wave vectors [11].

2.2 Solving for Oblique Spaces

For oblique spaces, the basis vectors of the fundamental domain must be defined and slanted. To start with the oblique 3-torus, we state its boundary conditions

of the tiling,

$$\xi_n(\mathbf{x}) = \xi_n(\mathbf{x} + \mathbf{T}). \tag{2.4}$$

Restated applying the spatial translation to the dual space,

$$e^{-i\mathbf{k}\cdot\mathbf{x}} = e^{-i\mathbf{k}\cdot\mathbf{x} - i\mathbf{k}\cdot\mathbf{T}}. \tag{2.5}$$

This gives us an expression the values of the successive wave vectors

$$\mathbf{k} \cdot \mathbf{T} = 2\pi n_a \tag{2.6}$$

which can be solved for

$$\mathbf{k} = 2\pi\mathbf{T}^{-1}(n_x, n_y, n_z) \tag{2.7}$$

This expression most generally gives the k dependence on spatial translations for any three-dimensional fundamental domain.

We must now solve for the $\mathbf{T}$ of the oblique torus topology though. The vector basis of this fundamental domain, $\hat{t}_1, \hat{t}_1$, and $\hat{t}_1$, can be specified by the dot products between them

$$\begin{aligned} \hat{t}_1 \cdot \hat{t}_2 &= L_x L_y \cos\theta_2 \\ \hat{t}_1 \cdot \hat{t}_3 &= L_x L_z \cos\theta_3 \\ \hat{t}_2 \cdot \hat{t}_3 &= L_y L_z(\sin(\theta_2)\sin(\phi_3) + \cos(\theta_2)\cos(\theta_3)) \end{aligned} \tag{2.8}$$

where θ_2, θ_3, and ϕ_3 are the angles of difference between basis vectors the first two basis vectors (t_1 is selected as z.) and θ_3 between the first and third.

These relationships define the T matrix, taking $\hat{t}_1$ to be $\hat{z}$,

$$T = \begin{pmatrix} 0 & 0 & L_1 \\ L_2\sin(\theta_2) & 0 & L_2\cos(\theta_2) \\ L_3\cos(\phi_3)\sin(\theta_3) & L_3\sin(\phi_3)\sin(\theta_3) & L_3\cos(\theta_3). \end{pmatrix} \tag{2.9}$$

As the oblique 3-torus does not have any flips in the connectedness of its domain, $\Gamma = T$ is its generator.

Because T is independent of the rotation component R of generators and the half and quarter-turn spaces share a fundamental domain with the oblique 3-torus, matrix 2.9 defines the spatial component their generators as well. This simplifies our computation of the eigenmodes of the oblique half-turn and oblique quarter-turn spaces to multiplying each of the $\mathbf{k}$ values produced by the rotation component of their generator by T^{-1}.

2.3 Candidate Space Solutions

2.3.1 Oblique 3-Torus

As mentioned above, the 3-torus has no rotation component of its generator and is only one planar wave. Therefore, the oblique 3-torus wave vector is given by

$$\begin{aligned} k_{x1} &= 2\pi\left(-\frac{n_x\cot(\theta_2)}{L_x}+\frac{n_y\csc(\theta_2)}{L_y}\right) \\ k_{z1} &= 2\pi\left(-\frac{n_x}{L_x}\right) \end{aligned} \tag{2.10}$$

and the intimidating

$$\begin{aligned} k_{y1} = 2\pi\Bigg(&-\frac{n_y\cot(\phi_3)\csc(\theta_2)}{L_y} \\ &+\frac{n_z\csc(\theta_3)\csc(\phi_z)}{L_z} \\ &+\frac{n_x\csc(\theta_2)\csc(\theta_3)\csc(\phi_3)L_yL_z(-\cos(\theta_3)\sin(\theta_2)+\cos(\theta_2)\cos(\phi_3)\sin(\theta_3))}{L_xL_yL_z}\Bigg) \end{aligned} \tag{2.11}$$

The full solution has the form

$$\xi_n^{(O3)}(\mathbf{x}) = e^{i\mathbf{k}_1\cdot\mathbf{x}} \tag{2.12}$$

2.3.2 Oblique Half Turn Space

To start with the half-turn torus, we require eigenmode solutions satisfying,

$$f(x,y,z) = f(-x,-y,z+L_z), \tag{2.13}$$

where the twist in the z dimension is chosen arbitrarily and L_z is the length of the fundamental domain in z. The generator which describes the next planar wave form in the linear combination is

$$R_a = \begin{pmatrix} -1 & 0 & 0 \\ 0 & -1 & 0 \\ 0 & 0 & 1 \end{pmatrix}. \tag{2.14}$$

This satisfies the above boundary conditions when applied to $\mathbf{k}$. With the T defined above, the corkscrew operation between tiles is defined for the half-turn space.

The terms of our solutions, planar waves, will be distinguished by the second term given by

$$\begin{aligned} k_{x1} &= 2\pi\left(\frac{n_x\cot(\theta_2}{L_x}-\frac{n_y\csc(\theta_2}{L_y}\right) \\ k_{z2} &= 2\pi\left(-\frac{n_x}{L_x}\right) \end{aligned} \tag{2.15}$$

and

$$k_{y1} = 2\pi \frac{n_y \cot(\phi_3)\csc(\theta_2)}{L_y} - \frac{n_z \csc(\theta_3)\csc(\phi_z)}{L_z} - \frac{n_x \csc(\theta_2)\csc(\theta_3)\csc(\phi_3) L_y L_z(-\cos(\theta_3)\sin(\theta_2) + \cos(\theta_2)\cos(\phi_3)\sin(\theta_3))}{L_x L_y L_z}. \tag{2.16}$$

This term is in addition to that of the standard oblique 3-torus. However, there is a spare term for the special case of $k_x = k_y = 0$, which is

$$k_{x3} = 0, \quad k_{y3} = 2\pi \left(\frac{2n_z \csc(\theta_3 \csc(\phi_3}{L_z} \right), \quad k_{z3} = 0, \tag{2.17}$$

which is preserved if and only if n_z is even.

Taken together, these two terms make the eigenmode of the half-turn space

$$\xi_n^{(H)}(\mathbf{x}) = \frac{1}{\sqrt{2}} \left(e^{i\mathbf{k}_1 \cdot \mathbf{x}} + (-1)^{n_z} e^{i\mathbf{k}_2 \cdot \mathbf{x}} \right) \text{ for } n_x \in Z^+, n_y, n_z \in Z \text{ or } n_x = 0, n_y \in Z^+, n_z \in Z. \tag{2.18}$$

and the spare, special case, eigenmode

$$e^{ik_3 \cdot x} \text{ for } n_z \in 2\mathbf{Z}. \tag{2.19}$$

2.3.3 Oblique Quarter Turn Space

The rotational component of the quarter turn topology's generator is

$$R_q = \begin{pmatrix} 0 & -1 & 0 \\ 1 & 0 & 0 \\ 0 & 0 & 1 \end{pmatrix}, \tag{2.20}$$

which switches k_x and k_y with a negation of the k_x dimension. The spatial translation by T_a is $\frac{L_a}{4}$, as our fundamental domain is again expanded to include the full modulus of rotations which bring the eigenmode planar wave terms back to $e^{\mathbf{k}_1 \cdot \mathbf{x}}$. Applying this generator repeatedly gives us four terms, two of which are identical to the terms of the half-turn space.

The first of the two wave vector terms unique to the quarter space is

$$k_{x4} = 2\pi \left(-\frac{n_x \cot(\theta_2}{L_x} - \frac{n_y \csc(\theta_2}{L_y} \right), \quad k_{z4} = 2\pi \left(\frac{n_y}{L_x} \right) \tag{2.21}$$

whose k_y value is still the cumbersome

$$k_{y4} = 2\pi \frac{n_y \cot(\phi_3)\csc(\theta_2)}{L_y} + \frac{n_z \csc(\theta_3)\csc(\phi_z)}{L_z} - \frac{n_x \csc(\theta_2)\csc(\theta_3)\csc(\phi_3) L_y L_z(-\cos(\theta_3)\sin(\theta_2) + \cos(\theta_2)\cos(\phi_3)\sin(\theta_3))}{L_x L_y L_z}. \tag{2.22}$$

The second eigenmode is given by $\mathbf{k}$

$$k_{x5} = 2\pi\left(\frac{n_x \cot(\theta_2)}{L_x} + \frac{n_y \csc(\theta_2)}{L_y}\right) \qquad k_{z5} = 2\pi\left(-\frac{n_y}{L_x}\right) \tag{2.23}$$

with k_y

$$k_{y5} = 2\pi \frac{n_y \cot(\phi_3)\csc(\theta_2)}{L_y} + \frac{n_z \csc(\theta_3)\csc(\phi_z)}{L_z} - \frac{n_x \csc(\theta_2)\csc(\theta_3)\csc(\phi_3) L_y L_z(-\cos(\theta_3)\sin(\theta_2) + \cos(\theta_2)\cos(\phi_3)\sin(\theta_3))}{L_x L_y L_z}. \tag{2.24}$$

This space still must denote a special case for the fixed case of $\mathbf{k} = (0, 0, k_z)$. In conclusion, the solution of the quarter solutions is the union of

$$\xi_n^{(Q)}(\mathbf{x}) = \frac{1}{2}\Big(e^{i\mathbf{k}_1\cdot\mathbf{x}} + i^{n_z} e^{i\mathbf{k}_2\cdot\mathbf{x}} + i^{2n_z} e^{i\mathbf{k}_4\cdot\mathbf{x}} + i^{3n_z} e^{i\mathbf{k}_5\cdot\mathbf{x}}\Big) \text{ for } n_x \in Z^+, n_y \in Z^+ \cup \{0\}, n_z \in Z \tag{2.25}$$

and the special case eigenmode

$$e^{ik_3\cdot z} \text{ for } n_z \in 4\mathbf{Z}. \tag{2.26}$$

Chapter 3

Generating the CMB Sky

3.1 Expansion in Terms of the Full-Sky

Building the pixel-pixel correlation matrix as described in Section 1.4.2 is an imposing computation problem, as there are on the order of 10^6 pixels in the Planck data [12] and suitable truncations must be placed on the $C_{pp'}$ expression's infinite sums. However, going to these lengths is unnecessary for extracting statistically significant observations from the CMB as there are often more pixels than independent CMB radiation modes carrying information about topological correlations in the full sky [8].

So instead, we shall expand the pixel-pixel correlation matrix entries in terms of a discrete set of mode functions orthonormal over the pixelized sphere (Similar to the approach of the Planck Collaboration in *Planck* 2013 Results XXVI [8].). In this case, we will use the eigenfunctions of $C_{pp'}$ on the full sphere with radius R_{LSS},

$$C_{pp'}\Psi_{p'}^{(\nu)} = \lambda_{(\nu)}^2\Psi_p^{(\nu)}. \tag{3.1}$$

As we shall see, this makes our computational task much easier.

The temperature at a position $\mathbf{x}$ on the full CMB sphere is best given in spherical coordinates

$$\Phi(\mathbf{x}) = \Phi(r, \Theta, \Psi) \tag{3.2}$$

where

$$\Phi(\mathbf{x}) = \sum_{j=1}^{\infty} a_j \xi_j(\mathbf{x}) \tag{3.3}$$

and the $\xi_j(\mathbf{x})$ terms are an orthonormal basis in which the temperature is expanded. Here, a good orthonormal basis is the spherical harmonics

$$\Phi(\mathbf{x}) = \sum_{n=1}\sum_{l=1}\sum_{m=1} a_{nlm} j_l(k_{nl}\,|r|)Y_{lm}(\Theta, \Psi). \tag{3.4}$$

because our examination is considering the full sky (The CMB without cuts.) and we are interested in angular scales much larger than the pixels.

Since we are considering a spherical surface of constant radius, the spherical Bessel function term $j_l(k_{nl}\,|r|)$ may be factored with the independent Gaussian random variable a_{nlm},

$$\Phi(\mathbf{x}) = \sum_{l=1}\sum_{m=1}\left[\sum_{n=1} a_{nlm} j_l(k_{nl} R_{\mathrm{LSS}})\right] Y_{lm}(\Theta,\Psi), \tag{3.5}$$

to define the temperature on the sphere as

$$\Phi(\mathbf{x}) = \sum_{l=1}\sum_{m=1} a_{lm} Y_{lm}(\Theta,\Psi). \tag{3.6}$$

The correlation matrix of the full sphere only then is given by

$$C_{pp'}^{\mathrm{Cov}} = \sum_{l=1}\sum_{m=1} C_l Y_{lm}(\hat{\mathbf{p}}) Y_{l'm'}(\hat{\mathbf{p}'}) \tag{3.7}$$

Although this expression of temperature in the observer frame does not by itself give us information regarding the topology, it serves as an eigenbasis for the topology frame correlation matrix because all observations of the topology frame actually occur in the observer frame. In other words, we have found a basis in the covering space out to the full CMB sky which the topology frame and observer frame share as

$$\Psi_p^{(\nu)} = Y_{lm}(\mathbf{p}) \tag{3.8}$$

by a bijective mapping between the νs and (l,m)s. This same mapping exists between the a_ns and the a_{lm}s.

3.2 Observable Mode-Mode Correlation Matrix

To make our observations, we will have to truncate the observed modes of the full sky to a useful yet computable number. In agreement with previous *Planck* correlation matrix searches, 837 modes are selected, corresponding to the number of modes on the full-sky up to $l_{\max} = 28$ spherical harmonic modes. This captures the most important topological correlation information of the pixel-pixel matrix in a manageable form.

Now, we have a 837×837 correlation matrix whose indices are the entries of our pixel-pixel correlation matrix expanded in terms of the spherical harmonic eigenfunctions described above,

$$C_{\nu\nu'} = \sum_{p=}^{N_p}\sum_{p'=1}^{N_p} C_{pp'} \Psi_\nu(\hat{p}) \Psi^*_{\nu'}(\hat{p}'). \tag{3.9}$$

Furthermore, the entries may be broken down into analytic integrals by splitting the two products of Laplacian eigenmodes (Which comprise $C_{pp'}$.) and

the Y_{lm}s the $C_{pp'}$ is expanded in terms of,

$$C_{\nu\nu'} = \sum_{n=1}^{\infty}\sum_{n'=1}^{\infty}\langle|a_n^2|\rangle\delta_{nn'}|\mathbf{k}_{nj}|^{-3}\left[\sum_{p=1}^{N_p}\xi_n(\hat{p})\Psi_\nu(\hat{p})\right]\left[\sum_{p'=1}^{N_p}\xi^*_{n'}(\hat{p'})\Psi^*_{\nu'}(\hat{p'})\right]. \tag{3.10}$$

Turning the two factors of equation 3.31 into integrals over pixel space gives us

$$I = \int \xi_n(\hat{p})\Psi_\nu(\hat{p})d\hat{p} = \int \xi_n(\hat{p})Y_{lm}(\hat{p})d^2\hat{p} \tag{3.11}$$

for each (To switch from one integral to another, we simply prime or unprime the pixel indices and take the complex conjugate.).

$$I = \sum_{n=1}\sum_{j=1}\xi_{nj}\int d^2\hat{p}Y_{lm}(\hat{p})e^{i\mathbf{k}_{nj}\cdot\mathbf{x}_p} \tag{3.12}$$

where the j index is once again selecting terms from the eigenmode's linear combination of plane waves.

To solve the integral, it helps to convert the plane waves of the topology frame to the spherical harmonics of the observer. The expansion of a plane wave in terms of spherical harmonics

$$e^{i\mathbf{q}\cdot\mathbf{v}} = \sum_{l=0}^{\infty} i^l\sqrt{4\pi(2l+1)}j_l(|q||v|)Y^*_{l0}(\frac{\mathbf{q}\cdot\mathbf{v}}{|q||v|}) \tag{3.13}$$

then defines an integral over only Y_{lm}s. After using the explicit form of x_p to factor out $e^{\mathbf{k}_{nj}\cdot\mathbf{r}_T}$ we have the integral

$$\begin{aligned} I = \sum_{n=1}\sum_{j=1}\xi_{nj}\sum_{l=0} i^l\sqrt{4\pi(2l+1)}j_l(|k_{nj}||R_{\mathrm{LSS}}|)e^{i\mathbf{k}_{nj}\cdot\mathbf{r}_T} \\ \cdot\int d^2\hat{p}Y_{lm}(\hat{p})Y_{l0}(\hat{k}_{nj}\cdot R_{\alpha\beta\gamma}\hat{p}) \end{aligned} \tag{3.14}$$

where j_l is the spherical Bessel function. j_l includes the radial description of the expanded plane wave in the observer frame while Y_{l0} includes the angular.

Equation 3.14 is an analytic integral. However, because we have expressed plane waves of many different forms at many different positions as spherical harmonics, we cannot easily relate the angular parameters of Y_{lm} to Y_{l0} yet - We must rotate their z-axes into alignment for the direction given by each $(\hat{k}_{nj}\cdot R_{\alpha\beta\gamma}\hat{p})$ argument. To do that, we'll change our integration variables.

To begin this translation, we introduce

$$\hat{q} = R^T_{\alpha\beta\gamma}\cdot\hat{k}_{nj} \tag{3.15}$$

which expresses the rotation in the Y_{l0} argument

$$\hat{k}_{nj}\cdot R_{\alpha\beta\gamma}\hat{p} = \hat{q}^T\cdot\hat{p} = \hat{q}\cdot\hat{p} \tag{3.16}$$

by simply including the orientation of a pixel with the product of the wave vector. Then, we rotate this $\hat{q}$ into alignment with the $\hat{z}$ axis with rotations about the x and y axis:

$$M(\theta_{1nj}, \theta_{2nj}, 0)\hat{q} = M(\theta_{1nj}, \theta_{2nj}, 0)(R^T_{\alpha\beta\gamma}\hat{k}_{nj}) = \hat{z} \tag{3.17}$$

where M is an x-y-z rotation matrix with angles θ_{1nj} about x and θ_{2nj} about y. Note the dependence of the angles on the direction of the $\hat{k}_{nj}$ vector they are aligning with $\hat{z}$, as well as on its respective Euler angles (α, β, γ).

We now have the Y_{l0} term from the plane wave expansion in a useful position, but the angle between $\hat{p}$ and $\hat{k}_{nj}$ must be preserved and Y_{lm} must be rotated into alignment with the Y_{l0}. So, we apply the M rotation to $\hat{p}$ of the Y_{l0}

$$Y_{l0}(\hat{q}^T[M^T M]\hat{p}) \tag{3.18}$$

such that its value is preserved by $M^T M = 1$. This still produces a $\hat{z}$ from $\hat{q}^T M^T$, but will introduce a new pixel variable we will call $\hat{\tilde{p}}$, the pixel rotated with respect to the alignment rotation of $\hat{q}$. This will be our new integration variable. Using the transpose of our rotation matrix M again, it appears in the Y_{lm} term as well,

$$\int d^2\hat{\tilde{p}} Y_{lm}(M^T\hat{\tilde{p}}) Y_{l0}(\hat{z} \cdot \hat{\tilde{p}}) \tag{3.19}$$

This allows us to integrate over both spherical harmonics while rotating the Y_{lm}.

Our last step is the actual rotation of Y_{lm} by the rotation M^T, given by

$$M(\omega_{nj}, \eta_{nj}, \phi_{nj}) = R^T(\theta_{1nj}, \theta_{2nj})R(\alpha, \beta, \gamma). \tag{3.20}$$

This rotation of Y_{lm} by $(\omega_{nj}, \eta_{nj}, \phi_{nj})$ is a function of θ_{1nj} and θ_{2nj}, the angles of alignment of q_{nj}, and α, β, and γ, the angles of orientation of $\hat{p}$ on the CMB sky.

It's worth showing how the angles of M are computed from these five rotations comprising the product $R^T(\theta_{1nj}, \theta_{2nj})R(\alpha, \beta, \gamma)$. Any z-y-z rotation [1] can be represented in a single matrix as the product of the three respective axis rotation matrices as

$$\begin{aligned} R &= R_{z_0}(a)R_y(b)R_{z_1}(c) \\ &= \begin{pmatrix} \cos(b)\cos(a)\cos(c) - \sin(a)\sin(c) & -\cos(c)\sin(a) - \cos(b)\cos(a)\sin(b) & \sin(b)\cos(a) \\ \cos(b)\cos(c)\sin(a) + \cos(a)\sin(c) & \cos(a)\sin(c) - \cos(b)\sin(a)\sin(c) & \sin(b)\sin(a) \\ -\sin(b)\cos(c) & \sin(b)\sin(c) & \cos(b) \end{pmatrix} \end{aligned} \tag{3.21}$$

with angles of rotation (a, b, c) for the first z rotation z_0, y rotation, and second z rotation z_1, respectively.

[1] The z-y-z Euler angle convention is used to ensure real valued $d^{(l)}_{mm'}(\beta)$ values when Wigner D-matrices are used to rotate Y_{lm}.

So, trigonometric identities between entries of the matrix may be used to find expressions for angles a, b, and c - Or in our case, ω_{nj}, η_{nj} and ψ_{nj}, the rotations angles of the z_0, y and z_1 axes respectively. Let the entries of matrix 3.21 be r_{ij}. The easiest angle is of course $\eta_{nj} = \arccos(r_{22})$, while the others are given by the arctangent of ratios of sine and cosine products which reduce to the corresponding expression for tangent,

$$\begin{aligned} \omega_{z_0,nj} &= \arctan\left(\frac{r_{12}}{r_{02}}\right) \\ \eta_{y,nj} &= \arccos(r_{22}) \\ \psi_{z_1,nj} &= \arctan\left(\frac{r_{21}}{-r_{20}}\right). \end{aligned} \tag{3.22}$$

However, in the cases $r_{22} = 1$ and $r_{22} = -1$ (When angle b is 0 and π.), $\sin(b) = 0$ defines both of the above inverse tangents with a division by 0. So, we must take advantage of the $\cos(b) = \pm 1$ terms and trigonometric angle sum and difference identites in the $0 \leq i \leq 1$, $0 \leq j \leq 1$ range of the matrix to define $\omega_{z_0,nj} + \psi_{z_1,nj} = \arctan\left(\frac{r_{10}}{r_{11}}\right)$ and $\omega_{z_0,nj} - \psi_{z_1,nj} = \arctan\left(\frac{r_{10}}{r_{11}}\right)$.

So these edge cases of the y rotation angle are expressed as

$$\begin{aligned} \omega_{z_0,nj} &= \begin{cases} -\arctan\left(\frac{r_{10}}{r_{11}}\right) \text{ if } r_{22} = -1 \\ \arctan\left(\frac{r_{10}}{r_{11}}\right) \text{ if } r_{22} = 1 \end{cases} \\ \eta_{y,nj} &= \begin{cases} \pi & \text{if } r_{22} = -1 \\ 0 & \text{if } r_{22} = 1 \end{cases} \\ \psi_{z_1,nj} &= 0. \end{aligned} \tag{3.23}$$

With our angle arguments, the Wigner D-matrices which rotate Y_{lm} are defined. The transpose of this rotation defines $Y_{lm}(M^T\hat{\hat{p}})$ in the integral

$$\int d^2\hat{\hat{p}} Y_{lm}(M^T\hat{\hat{p}}) Y_{l0}(\hat{z}^T \cdot \hat{\hat{p}}). \tag{3.24}$$

The rotation of the Y_{lm} must be expressed as the sum

$$\sum_{m'=-l}^{l} D^{(l)}_{mm'}(\omega_{x,nj}, \eta_{y,nj}, \psi_{x,nj}) Y_{lm}(\hat{\hat{p}}) \tag{3.25}$$

where $D^{(l)}_{mm'}$ is the respective index of the square $(2l+1)$ Wigner D-Matrix given by

$$D^{(l)}_{mm'}(\alpha, \beta, \gamma) = e^{-im'\alpha} d^{(l)}_{m'm}(\beta) e^{im\gamma} \tag{3.26}$$

where Wigner's 'small' d-matrix is

$$\begin{aligned} &d^{(l)}_{m'm}(\beta) = \left[(j+m')!(j-m')!(j+m)!(j-m)!\right]^{1/2} \cdot \\ &\sum_s \left[\frac{(-1)^{m-m'+s}}{(j+m-s)!s!(m'-m+s)!(j-m'-s)!} \cos(\frac{\beta}{2})^{2j+m-m'-2s} \sin(\frac{\beta}{2})^{m'-m+2s} \right]. \end{aligned} \tag{3.27}$$

Now, the orthogonality of the spherical harmonics is a joy to behold. Extracting the $D^{(l)}_{mm'}$ term from the integral gives

$$\sum_{m'} D^{(l)}_{mm'}(\omega_{x,nj}, \eta_{y,nj}, \psi_{x,nj}) \int d^2\hat{\tilde{p}} Y_{lm}(\hat{\tilde{p}}) Y_{l0}(\hat{\tilde{p}}), \tag{3.28}$$

whose integral is the Dirac-Delta function $\delta_{m'0}$ by the orthogonality of the Y_{lm}s. This too reduces the sum of $D^{(l)}_{mm'}$s to

$$\sum_{m'} D^{(l)}_{mm'}(\omega_{x,nj}, \eta_{y,nj}, \psi_{x,nj})\delta_{m0} = D^{(l)}_{0m}(\omega_{x,nj}, \eta_{y,nj}, \psi_{x,nj}) \tag{3.29}$$

The solution for the integral of the full sphere Y_ν eigenfunctions and the ξ_ν Laplacian eigenmode solutions of equation 3.11 is then

$$I = \sum_{n=1}\sum_{j=1}\xi_{nj}\sum_{l=0} i^l\sqrt{4\pi(2l+1)}\cdot \\ j_l(|k_{nj}||R_{\rm LSS}|)e^{i\mathbf{k}_{nj}\cdot\mathbf{r}_T} D^{(l)}_{0m'}(\omega_{x,nj}, \eta_{y,nj}, \psi_{x,nj}). \tag{3.30}$$

When multiplied by its complex conjugate and appropriate C_n (And its n eigenmode sum is extracted over the C_n.),

$$C_{\nu\nu'} = \sum_{n=1}^{\infty}\sum_{n'=1}^{\infty}\langle|a_n^2|\rangle\delta_{nn'}|\mathbf{k}_{nj}|^{-3} I_\nu(\xi_n, Y_{lm}) I^*_{\nu'}(\xi_{n'}, Y_{l'm'}). \tag{3.31}$$

These integrals, when numerically computed, will be marginalized spatially over the compactification parameters (L_x, L_y, L_z) and oblique angles (A_x, A_y, A_z) of a space which distinguish the terms of ξ_n.

Chapter 4

Summary

In this senior project and report, we have laid the foundational tools and references for future work actually comparing anticipated CMB correlations with observed Planck data for signatures of non-trivial topologies. This was done in two parts.

First, we have researched and compiled the Laplacian eigenmodes of 3 oblique spaces. These eigenmodes uniquely characterize the correlations in the CMB angular power spectrum for each respective space and have not been examined in previous cosmic topology searches. They trivially work for all angles of obliqueness and, as the simplest cases of oblique spaces, would be the first tests of an oblique torus topology search.

More importantly, we have defined a correlation matrix computation for simulating the two-point correlation function of any candidate space. This method is robust, efficient, and modular so that it may quickly and simply incorporate new spaces as their solutions are derived and the work of Prof. Starkman and his collaborators is extended.

While these derivations have not yet been compared to Planck data with a likelihood function to search for signatures of a multiconnected cosmic topology, they will form the basis of future work.

Bibliography

[1] Levin, Janna. "Topology and the Cosmic Microwave Background", arXiv:gr-qc 0108043v2 20 Aug 2001

[2] Watson, Laura J. "Signatures of Cosmic Topology in the Polarised Cosmic Microwave Background", Doctor of Philosophy Thesis, Imperial College London, 2014

[3] [arXiv:astro-ph/0310233]

[4] Neil J Cornish et al, 1998 Class. Quantum Grav. 15 2657. doi:10.1088/0264-9381/15/9/013

[5] Hitchman, Michael P., Geometry with an Introduction to Cosmic Topology. Sudbury, MA: Jones and Bartlett, 2009. Print.

[6] Pascal M. Vaudrevange, Glenn D. Starkman, Neil J. Cornish, David N. Spergel , 2012, arXiv:1206.2939v1 [astro-ph.CO]

[7] Neil J. Cornish, David N. Spergel, Glenn D. Starkman, Eiichiro Komatsu, 2003, [arXiv:astro-ph/0310233]

[8] Planck Collaboration XXVI., Background Geometry and Topology of the Universe, 2014, [arXiv:astro-ph/1303.5062]

[9] G.I. Gomero, M.J. Rebou A.F.F. Teixeira, Spikes in cosmic crystallography II: topological signature of compact flat universes, 2014, arxiv-gr-qc9909078

[10] Canzani, Yaiza. "Notes on Analysis on Manifolds via the Laplacian", Math 253, Harvard University, Fall 2013

[11] Riazuelo, et al. "Cosmic microwave background anisotropies in multiconnected flat spaces" Physical Review D 69, 103518. 2004

[12] Krzysztof M. Gorski, Benjamin D. Wandelt, Eric Hivon, Frode K. Hansen, and Anthony J. Banday. "The HealPix Primer", http://healpix.jpl.nasa.gov/pdf/intro.pdf, June 18, 2010